

Phase Crossover induced by Dynamical Many Body Localization in Periodically Driven Long-Range Spin Systems

Mahbub Rahaman,¹ Takashi Mori,² and Analabha Roy^{1,*}

¹Department of Physics, The University of Burdwan, Golapbag, Bardhaman - 713 104, India

²RIKEN CEMS, 2-1 Hirosawa, Wako, Saitama, 351-0198, Japan

Dynamical many-body freezing occurs in periodic transverse field-driven integrable quantum spin systems. Under resonance conditions, quantum dynamics causes practically infinite hysteresis in the drive response, maintaining its starting value. We extended this to non-integrable many-body systems by reducing the Hamiltonian symmetries through a power-law dependence in spin exchange energy, $J_{ij} = 1/|i - j|^\beta$. The dynamics of the integrable short-range Transverse Field Ising Model (TFIM) and non-integrable long-range Lipkin Meshkov Glick (LMG) models were investigated. In the LMG, the resonance conditions in the driving field suppresses the heating postulated by the *Eigenstate Thermalization Hypothesis* (ETH) by inducing *Dynamical Many Body Localization*, or DMBL. This is in contrast to Many Body Localization (MBL), which requires disorder to suppress ETH. DMBL has been validated by the Inverse Participation Ratio (IPR) of the quasi-stationary Floquet modes. While TFIM has IPR localization for all drive parameters, the LMG exhibits high-frequency localization only at the resonances. IPR localization in the LMG deteriorates with an inverse system size law at lower frequencies, which indicates heating to infinite temperature. Furthermore, adiabatically increasing frequency and amplitude from low values raises the Floquet state IPR in the LMG from nearly zero to unity, indicating a phase crossover. This occurrence enables a future technique to construct an MBL engine in clean systems that can be cycled by adjusting drive parameters only.

Keywords: Dynamical localization, Thermalization, Phase Crossover

Under certain resonance conditions in the drive parameters, periodically driven quantum many-body systems can experience dynamical many-body freezing (DMF), which causes the response to freeze completely to its initial value at all times [1–3]. This arises as a consequence of additional approximate symmetries that occur at resonance. DMF has been demonstrated via the Rotating Wave Approximation (RWA) in the driven TFIM with nearest-neighbour interactions [4] and is shown to be protected when translational invariance is explicitly broken (say, by disorder) [5, 6].

The utilization of Floquet theory simplifies the analysis of time-periodic systems. For closed quantum systems governed by the time-dependent Schrödinger equation, the *Floquet Hamiltonian* allows for a mapping of the time-dependent dynamics into the dynamics of a time-independent effective Hamiltonian, provided the system is strobed at integer multiples of the time period of the drive. The time independent eigenstates of the effective Hamiltonian correspond to quasi-stationary *Floquet Modes* of the original Hamiltonian. The temporal progression of the system comes from phase coefficients that capture the dynamics [7, 8].

Any sufficiently complex non-integrable Many Body System is expected to thermalize according to the Eigenstate Thermalization Hypothesis (ETH) despite

the fact that closed quantum dynamics preserves the memory of the initial state of the system. This arises due to the properties of the matrix elements of observables in typical states[9]. The ETH can be readily adapted to time-periodic systems using Floquet theory (the Floquet-ETH, or FETH). Nonetheless, the conditions for ETH to hold are not particularly strong, and the density matrix of the system can fail to approach one that is described by a thermal expression. Thermal systems must conduct because they exchange energy and particles internally during thermalization. Thus, insulating systems can be naturally athermal; Many Body Localization (MBL) is a well-studied case [10]. This phenomenon is stable against local perturbations, and constitutes an exotic state of matter with far-reaching implications in theoretical physics, as well as in practical applications[11].

The addition of disorder has been identified as a crucial component in the onset of MBL. In that case, thermalization is prevented by disorder-induced localization. Nonetheless, alternative approaches to MBL in strongly interacting disorder-free systems [12–14], inhomogeneous systems [15–18], and by inducing disorder in the emergent physics [19] and by other effective means [17] (albeit with strong finite-size effects), have been reported. An alternative approach to realizing MBL in disorder-free homogeneous many-body systems involve *Floquet Engineering*, where a time-periodic drive is introduced, and the drive parameters tuned to introduce a clustering of quasistationary en-

* Email:daneel@utexas.edu

64 ergies in a manner similar to localization[9].

65 In this article, we use the fact that emergent ap-
66 proximate symmetries can be engineered in Floquet
67 systems and apply it to long-range interactions. This
68 results in *Dynamical Many Body Localization* (DMBL)
69 at resonant values of the drive parameters, and com-
70 plete thermal behaviour at other values. This phe-
71 nomenon is distinct from DMF in the TFIM, since
72 clean TFIM systems, being integrable, never thermal-
73 ize.

74 To demonstrate the onset of MBL, we investigate
75 the driven Lipkin-Meshkov-Glick (LMG) model[20-
76 25], a long-range system that extends the nearest-
77 neighbour interactions in the TFIM to all-to-all inter-
78 actions. [26-28] We have recovered the onset of DMF
79 in this system and have supported our result with nu-
80 matical simulations.

81 In addition, we compare the degree of localization
82 of the quasi-stationary Floquet modes in the LMG
83 model with the TFIM. In order to do so, we look at the
84 Inverse Participation Ratio (IPR) of the Floquet modes
85 in the representation given by the eigenstates of the
86 symmetry-breaking field. The IPR, closely related to
87 the concept of quantum purity, is defined as the formal
88 sum of the square of the density in some physically
89 meaningful space or representation. A high IPR of a
90 stationary state denotes low participation in most of
91 the representation, and a low IPR distributes partic-
92 ipation uniformly across the representation, leading
93 to ergodic dynamics[29]. Thus, IPR [30] is a useful
94 tool for witnessing MBL of a quantum system. For an
95 MBL system, the IPR is unity, and it scales inversely
96 with the number of spins when it is thermally dis-
97 tributed [31].

98 In the first section of this paper, we present all es-
99 sential theoretical frameworks. Our results for the
100 LMG model are presented next in section II. In that
101 section, we have used the Rotating Wave Approx-
102 imation (RWA) [32], where only the slowest rotating
103 terms in the Fourier expansion of the Hamiltonian in
104 a frame co-rotating with the symmetry breaking drive
105 field are retained. In addition, we have obtained
106 numerical simulations of the Floquet modes and their
107 IPR. They are used to probe the system dynamics in
108 the high and low-frequency domains at both limits of
109 β . In section III we have used phase space plots to
110 contrast the low and high frequency limits of the LMG
111 model in the thermodynamic limit by mapping it to an
112 equivalent classical Hamiltonian system. Finally, in
113 section IV, we have looked at numerical computations
114 of the IPR of the Floquet modes for different values of
115 the drive parameters, well beyond those that allow for
116 the RWA. We observed that, if the system is driven by
117 an adiabatically increasing drive frequency from low
118 to high limit while remaining in the resonance region,

119 a sharp crossover from a thermal to an MBL phase
120 occurs. We conclude with discussions and outlook.

I. BACKGROUND

122 The Eigenstate Thermalization Hypothesis (ETH) is
123 a series of conjectures that allows for the thermaliza-
124 tion of an isolated quantum many body system. The
125 state of the system, $|\psi(t)\rangle$, evolves according to the
126 Schrödinger equation $\hat{H}|\psi(t)\rangle = i\frac{\partial}{\partial t}|\psi\rangle$. The Hamilto-
127 nian \hat{H} is assumed to be *non-integrable*, in that it lacks
128 an extensive number of conserved quantities that can
129 be written as a sum of local operators, that is to say,
130 there are no set of observables $\hat{O}_s = \sum_i \hat{L}_i$ such that
131 $[\hat{O}_s, \hat{H}] = 0$. Here, the \hat{O}_s constitute an arbitrary
132 CSCO (complete set of commuting observables), and
133 \hat{L}_i are *local*, each having sub-extensive support in the
134 system [33]. In addition, we postulate an "equilib-
135 rium" value A_{eq} for every observable \hat{A} , such that

$$A_{eq}(E) \equiv \frac{\text{Tr}(\hat{A}e^{-\beta\hat{H}})}{\text{Tr}(e^{-\beta\hat{H}})}, \quad (1)$$

136 where $E = \langle\psi(t)|\hat{H}|\psi(t)\rangle$ is the conserved energy of
137 the system, and $\beta = 1/(k_B T)$ is the inverse tempera-
138 ture, H_{eq} is an effective Hamiltonian that captures the
139 long-time average dynamics of the system, and k_B is
140 the Boltzmann constant.

To put it simply, ETH proposes that this many-
body Hamiltonian undergoes thermalization as seen
in the *long-time averages* of observables, with the
eigenstates bearing resemblance to thermal states.
The aforementioned hypothesis serves as a valuable
instrument for comprehending the conduct of stim-
ulated quantum systems and their correlation with
thermal equilibrium. This assertion can be justified
by examining the expectation value of an observable
 \hat{A} as it evolves under the Schrödinger equation. To
see this, we first expand the state of the system $|\psi(t)\rangle$
as:

$$|\psi(t)\rangle = \sum_m c_m(t) |m(0)\rangle,$$

141 where $|m(0)\rangle$ represents the eigenstates of $\hat{H}(0)$ with
142 energy E_m . The coefficients $c_m(t)$ describe the time-
143 dependent amplitude of the expansion. Plugging
144 these expansions into the expression for the expec-
145 tation value, we obtain the long-time average of the
146 expectation value [34]:

$$\overline{\langle \hat{A}(t) \rangle} = \sum_{m,k} \overline{c_m^*(t)c_k(t)} \langle m(0)|\hat{A}|k(0)\rangle, \quad (2)$$

¹⁴⁷ where the overline indicates the following operation
¹⁴⁸ for any time-dependent quantity $\mathcal{O}(t)$,

$$\overline{\mathcal{O}} \equiv \lim_{t \rightarrow \infty} \frac{1}{t} \int_0^t d\tau \mathcal{O}(\tau). \quad (3)$$

The matrix elements $\langle m(0) | \hat{A} | k(0) \rangle$ are said to satisfy the Srednicki ansatz [35, 36]:

$$\begin{aligned} \langle m(0) | \hat{A} | k(0) \rangle &\approx A_{eq} \left(\frac{E_m + E_k}{2} \right) \delta_{mk} + \\ &e^{-\frac{1}{2}S\left(\frac{E_m+E_k}{2}\right)} f \left(\frac{E_m + E_k}{2}, E_m - E_k \right) R_{mk}. \end{aligned} \quad (4)$$

Here, S is the thermodynamic entropy and R_{mk} are elements of a random matrix with vanishing mean and unit variance. What this means for the ensuing dynamics is that the system explores the accessible Hilbert space uniformly, and the matrix elements $\langle m(0) | \hat{A}(t) | k(0) \rangle$ become indistinguishable for most pairs of m and k . Applying this ansatz and taking the thermodynamic limit by ignoring terms $\mathcal{O}(e^{-S/2})$, the expression for the expectation value becomes:

$$\begin{aligned} \overline{\langle \hat{A}(t) \rangle} &\approx \sum_m \overline{|c_m(t)|^2} A_{eq}(E_m) \\ &\approx A_{eq}(E) \sum_m \overline{|c_m(t)|^2} = A_{eq}(E), \end{aligned}$$

¹⁴⁹ where, in the last step, we utilized the fact that A_{eq} is
¹⁵⁰ a smooth function, and that the states with energies
¹⁵¹ far from E have $|c_m(t)|^2 \approx 0$. Therefore, in the limit of
¹⁵² large systems the expectation value of an observable
¹⁵³ \hat{A} is approximately equal to the thermal expectation
¹⁵⁴ value A_{eq} . This is the essence of the ETH, which sug-
¹⁵⁵ gests that individual eigenstates of a quantum system
¹⁵⁶ can be described by statistical mechanics in the long-
¹⁵⁷ time limit.

¹⁵⁸ We now generalize the ETH to non-integrable many
¹⁵⁹ body systems that are closed, but not isolated. In
¹⁶⁰ that case, it is possible to impart a periodic time-
¹⁶¹ dependence on the Hamiltonian while still ensuring
¹⁶² unitary evolution. If the time period of the drive
¹⁶³ is T , and the corresponding drive frequency $\omega \equiv$
¹⁶⁴ $2\pi/T$, the Floquet theorem states that the solutions to
¹⁶⁵ the Schrödinger equation can be written as $|\psi(t)\rangle =$
¹⁶⁶ $e^{-i\epsilon t/\hbar} |\phi(t)\rangle$, where the $|\phi(t)\rangle$ are T -periodic states
¹⁶⁷ called *Floquet Modes*, the corresponding $\epsilon \in \mathbb{R}$, are
¹⁶⁸ called *quasienergies*. Quasienergy values are not
¹⁶⁹ unique, and can be made to be bounded within a Flo-
¹⁷⁰ quet Brillouin zone, viz. a range $[-\omega/2, \omega/2]$ [37, 38].
¹⁷¹ As a consequence, the unitary evolution operator can
¹⁷² be split into two parts as follows [39].

$$U(t) = e^{-i\hat{K}_F(t)} e^{-i\hat{H}_F t}. \quad (5)$$

¹⁷³ Here, the micromotion operator $\hat{K}_F(t)$ is time-periodic
¹⁷⁴ in T , with $\hat{K}_F(0) = 0$, and the Floquet Hamiltonian
¹⁷⁵ $\hat{H}_F = e^{i\hat{K}_F(t)} [\hat{H}(t) - i\partial_t] e^{-i\hat{K}_F(t)}$. Thus, if the sys-
¹⁷⁶ tem is strobed at integer multiples of T only, then
¹⁷⁷ the unitary evolution matches that of a time inde-
¹⁷⁸ pendent Hamiltonian H_F . This can capture most of
¹⁷⁹ the exact dynamics at large frequencies. In such sys-
¹⁸⁰ tems, the *Floquet Eigenstate Thermalization Hypo-*
¹⁸¹ *thesis* (FETH) posits that, subject to specific conditions
¹⁸² and in the context of a system of significant size, the
¹⁸³ Floquet modes themselves exhibit thermal state-like
¹⁸⁴ behavior, i.e., $\hat{H} \approx \hat{H}_F$ in eqn 1. However, in contrast
¹⁸⁵ to the isolated systems, the loss of energy conserva-
¹⁸⁶ tion allows for the mixing of all Floquet modes in the
¹⁸⁷ ensuing dynamics, not just those with quasienergies
¹⁸⁸ near E . Were this to actually happen in the ensuing
¹⁸⁹ dynamics, it can be reconciled with ETH by ensuring
¹⁹⁰ that the RHS of eqn 1 is independent of β , i.e., an
¹⁹¹ infinite temperature ensemble [40]. In other words,
¹⁹² the nonequilibrium steady state of the system tends
¹⁹³ to an infinite temperature, maximum entropy density
¹⁹⁴ matrix.

¹⁹⁵ However, drive parameters like amplitude, fre-
¹⁹⁶ quency, and duty-cycle strongly affect the structure
¹⁹⁷ of the Floquet modes $|\phi\rangle$. Thus, they can be engi-
¹⁹⁸ neered to prevent the kind of full mixing that would
¹⁹⁹ lead to infinite temperatures, manifesting suppres-
²⁰⁰ sion of thermalization dynamically. Thus, this type
²⁰¹ of *Floquet Engineering* can produce *Dynamical Many*
²⁰² *Body Localization* (DMLB), where the system fails
²⁰³ to reach thermal equilibrium and remains localized,
²⁰⁴ possibly near its initial state, even at large times.
²⁰⁵ This paradigm seems similar to standard Many-Body
²⁰⁶ Localization [41, 42], where disorder, locality, and inte-
²⁰⁷ grability can cause athermalism via breakdown in the
²⁰⁸ Srednicki ansatz. However, DMLB stems from peri-
²⁰⁹ odic driving, and thus can occur regardless of disor-
²¹⁰ der, locality of observables, or system integrability, all
²¹¹ of which have been studied for MBL onset [41, 43, 44].

Integrable Many Body systems do not exhibit thermalization. When subjected to time-periodic drives, Floquet engineering allows for the introduction of additional approximate conserved quantities that dynamically suppress the evolution of certain observables by hysteresis. This type of *freezing* of response has been shown in integrable systems [6]. A paradigmatic example is the driven Transverse Field Ising model (TFIM) in one dimension [45]. The Hamiltonian

is given by

$$\hat{H}(t) = \hat{H}_0 + h_z(t) \hat{H}_1, \quad (6)$$

$$\hat{H}_0 = -\frac{1}{2} \sum_{i=1}^N \sigma_i^x \sigma_{i+1}^x, \quad (7)$$

$$\hat{H}_1 = -\frac{1}{2} \sum_{i=1}^N \sigma_i^z. \quad (8)$$

Here, the undriven Hamiltonian \hat{H}_0 consists of nearest-neighbour interactions between N number of spin-1/2 particles on a one-dimensional spin network. The transverse field is denoted by \hat{H}_1 , and is being varied by a time-periodic and harmonic signal $h_z(t) = h_0 + h \cos \omega t$, yielding a time period $T = 2\pi/\omega$ with amplitude h , drive frequency ω , and d.c. field h_0 . This Hamiltonian can be readily transformed into a spinless pseudo-fermionic system via the Jordan-Wigner transformation [4]. When written in momentum space spanned by spinors $\psi_k = (c_{-k}, c_k^\dagger)^T$ of fermions at momentum k created (annihilated) by operators c_k^\dagger (c_k), the effective Hamiltonian

$$H(t) = \sum_{(k,-k)-\text{pairs}} \psi_k^\dagger \left[\left(f_k - h_z(t) \right) \tau_z + \tau_x \Delta_k \right] \psi_k, \quad (9)$$

where $f_k = \cos k$, $\Delta_k = \sin k$, τ_{xyz} are the three Pauli Matrices, and the sum is over distinct $(k, -k)$ Cooper Pairs. We can transform our system to a frame that rotates with the time-varying symmetry-breaking field. This is achieved by the means of the unitary transformation operator

$$U(t) = \prod_k U_k(t) \quad (10)$$

$$U_k(t) = \exp \left\{ \left[\frac{i\hbar}{\omega} \sin \omega t \right] \tau_z \right\}.$$

The resulting transformed Hamiltonian $H'(t) = U^\dagger(t) H(t) U(t) - iU^\dagger(t) \partial_t U(t)$ simplifies to

$$H'(t) = \sum_{(k,-k)-\text{pairs}} \psi_k^\dagger \left[\tau_z f_k + \tau_x \cos(\eta \sin \omega t) + \tau_y \sin(\eta \sin \omega t) \right] \psi_k, \quad (11)$$

where we defined $\eta = 2h/\omega$. Using the Jacobi-Anger formula [46]

$$e^{i\eta \sin \omega t} = \sum_{n=-\infty}^{\infty} J_n(\eta) e^{in\omega t}, \quad (12)$$

where $J_n(\eta)$ are Bessel Functions, the transformed Hamiltonian simplifies to

$$H'(t) = \sum_{(k,-k)-\text{pairs}} \psi_k^\dagger \left\{ \tau_z f_k + 2\tau_x \Delta_k \sum_{n \geq 0} J_{2n}(\eta) \cos(2n\omega t) - 2\tau_y \Delta_k \sum_{n \geq 0} J_{2n+1}(\eta) \sin[(2n+1)\omega t] \right\} \psi_k. \quad (13)$$

In the frequency regime $\omega \gg f_k$, the long-time average $H^{RWA} \equiv \lim_{n \rightarrow \infty} \frac{1}{nT} \int_0^{nT} dt H'(t)$ can serve as a suitable approximation for $H'(t)$. This approximation, known as the *Rotated Wave Approximation* (RWA), eliminates the oscillating modes and results in an effective Hamiltonian that is independent of time,

$$H^{RWA} = \sum_{(k,-k)-\text{pairs}} \psi_k^\dagger \left[f_k \tau_z + 2J_0(\eta) \Delta_k \tau_x \right] \psi_k. \quad (14)$$

It is evident that by manipulating the drive parameters, specifically the amplitude denoted by h and the frequency denoted by ω , in a manner such that η is positioned on a root of $J_0(\eta)$, the fermion number can be conserved to a significant extent at this particular resonance. Consequently, it is feasible to exercise direct control over H^{RWA} , resulting in a comprehensive suppression of the dynamics of otherwise responsive observables.

This phenomenon is highly general in nature, and can be readily adapted to non-integrable systems. In such cases, freezing has the additional effect of inducing DMBL, suppressing thermalization to infinite temperatures. Numerical quantification of localization of a specific (quasi) stationary state in a physically significant representation can be achieved through the computation of the *Inverse Participation Ratio* (IPR). The IPR is generally defined as the formal sum over the square of the local density in a physically meaningful space. [47–50] In the single particle case, the IPR, for a state $|\psi\rangle$ can be written as

$$\phi_{IPR} \equiv \int dx |\langle x | \psi \rangle|^4.$$

This definition can be applied to obtain the IPR of a state $|\phi\rangle$ in a representation given by any single particle basis $|m\rangle$ as

$$\phi_{IPR} \equiv \sum_m |\langle m | \psi \rangle|^4. \quad (15)$$

The smallest value of the IPR corresponds to a fully de-localized state, $\psi(x) = 1/\sqrt{N}$ for a system of size N [50, 51]. Values of the IPR close to unity correspond to localized states [30]. For a periodically driven system, we look at the IPR of the quasi-stationary Floquet

250 modes at $t = T$, where $t = 2\pi/\omega$ for drive frequency ω .
 251 In the TFIM model, equation 14 indicates that, at reso-
 252 nance, when $J_0(\eta) = 0$, the Floquet modes are approx-
 253 imately given by the fermionic Fock states, which have
 254 a trivially unit IPR in the representation of the eigen-
 255 modes of the transverse field \hat{H}_1 in equation 6. Here, a
 256 particular Floquet mode can be decomposed into a di-
 257 rect product of cooper-pair states as $|\phi\rangle = \prod_{k,-k} |\phi_k^n\rangle$.
 258 In the RWA limit and at resonance, $|\phi_k^n\rangle$ has values of
 259 $|0\rangle, |k, -k\rangle$ for two values of $n = 0, 1$ respectively. We
 260 define the reduced IPR of $|\phi_k^n\rangle \forall k$ to be

$$\phi_{IPR}^{(n)}(k) = |\langle 0|\phi_k^n\rangle|^4 + |\langle +k, -k|\phi_k^n\rangle|^4, \quad (16)$$

261 where $n = 0, 1$. The full many-body IPR can be ob-
 262 tained from the reduced IPR in eqn 16 by a product
 263 over all momenta in the Brillouin zone, yielding

$$\phi_{IPR} = \prod_k \phi_{IPR}^{(n)}(k). \quad (17)$$

264 In the RWA limit and at resonance , this quantity is
 265 unity, indicating very low participation and the onset
 266 of freezing. Figure 1 shows results from numerically
 267 simulating the TFIM dynamics. The reduced IPR for a
 268 particular Floquet mode recovered by simulating the
 269 exact Schrödinger dynamics over a single time period
 270 of the drive, and plotted as a function of momentum k
 271 for different η 's. At resonance, when η lies at the root
 272 of the Bessel function $J_0(\eta)$, the Reduced IPR is nearly
 273 unity for all momenta. Consequently, so is ϕ_{IPR} . Out-
 274 side this resonance, the IPR is unity only for some mo-
 275 ments because the effective Hamiltonian is perfectly
 276 diagonal at $k \in \{-\pi, 0, \pi\}$ as can be seen in the cross-
 277 sectional plots of figure 1. As we move away from the
 278 resonance point, the full IPR decreases exponentially
 279 as a power law in the system size, as can be seen in the
 280 bottom-right panel of fig 2 However, as the TFIM is an
 281 integrable spin model, the IPR never drops to a value
 282 that is small enough to indicate thermalization. This
 283 can be seen in the bottom panels of figure 2, where
 284 the power-law decay of $\phi_{IPR}(N)$ never approaches the
 285 thermodynamic scaling law $\phi_{IPR}(N) \sim 2^{-N}$ for either
 286 small or large frequencies. Note that, at low frequen-
 287 cies, RWA complete localization fails due to the un-
 288 availability of zero off-diagonal terms in the effective
 289 transformed Hamiltonian, as well as the absence of
 290 integrability breaking terms to counteract the off di-
 291 agonal terms. Because the TFIM can be mapped to a
 292 system of noninteracting particles as shown in eqn 9,
 293 it is not physically meaningful to refer to the unit IPR
 294 region as "Many Body Localization", because the pa-
 295 rameter space lacks a thermalized region to contrast
 296 with this state. The type of Floquet Engineering de-

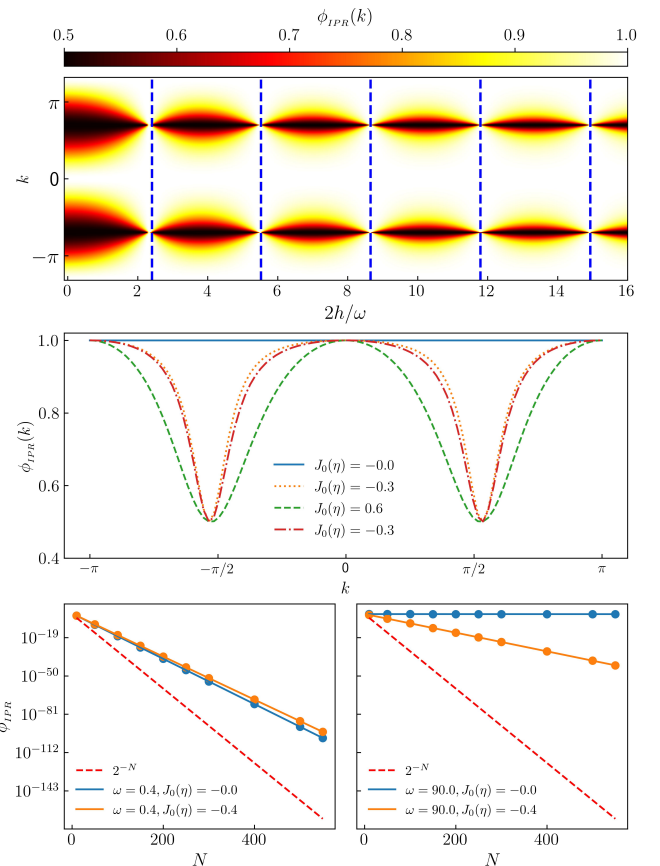


FIG. 1. Reduced IPR (defined in equation 16) for one of the two Floquet modes obtained from the exact dynamics of the TFIM for size $N = 100, \omega = 90$ for the entire Brillouin zone (top panel, ordinate) and a few drive amplitudes (top panel, abscissa). The dashed lines (top panel) indicate the roots of $J_0(\eta)$. The middle panel shows cross-sections of the reduced IPR in k -space for four chosen amplitudes. Finally, the bottom panels show semi-log plots of the scaling with N of the full many body IPR as defined in eqn 17, with the left panel for a small $\omega = 0.4$, amplitude h chosen to lie both in and out of the root of $J_0(\eta)$ as indicated in the legend, with similar plots on the right panel for a large $\omega = 90$.

307 FETH is expected to hold in certain regions. Long-
 308 range spin systems, in particular, where the exchange
 309 energies between far-off spins are taken into account
 310 in the model Hamiltonian, are good candidates be-
 311 cause they are known to thermalize when driven with
 312 low frequencies [52].

II. LONG RANGE INTERACTIONS: THE LIPKIN MESHKOV GLICK MODEL:

The periodically driven Lipkin Meshkov Glick (LMG) model [20, 53] for N long-range spins is described by

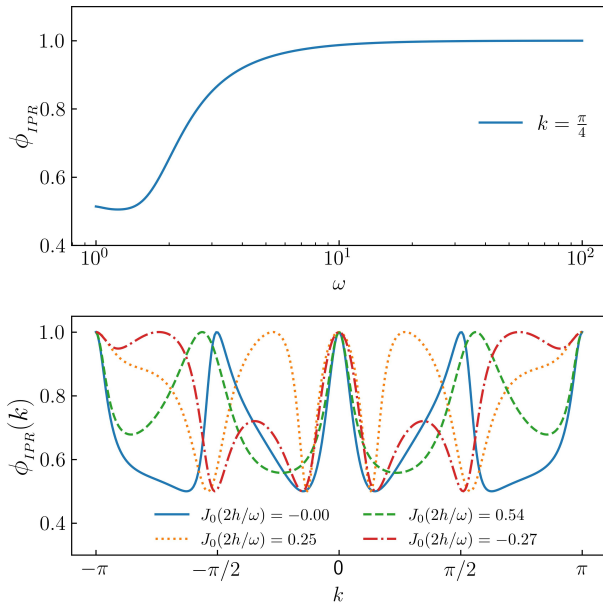


FIG. 2. Reduced IPR obtained by adiabatically increasing ω (top panel abscissa) for one the floquet mode obtained from equation 16 at the root of $J_0(\eta)$ for $N = 500$. IPR is ~ 0.5 (localized yet not fully freezing) upto $\omega \sim 2$, after that, smoothly increased to unity (fully localized and freezing) at higher $\omega \geq 10$ (top panel, ordinate). At bottom panel cross-sections for four chosen amplitudes at $\omega = 2$ are plotted for a brillouin zone (abscissa) with corresponding reduced IPRs (ordinate).

³¹¹ the Hamiltonian

$$\hat{H}(t) = \hat{H}_0 + [h \cos(\omega t) + h_0] \hat{H}_1. \quad (18)$$

³¹² Here, the undriven part \hat{H}_0 and the driven part \hat{H}_1 are,
³¹³ respectively,

$$\begin{aligned} \hat{H}_0 &= \frac{2}{N-1} \sum_{ij} \hat{\sigma}_i^z \hat{\sigma}_j^z, \\ \hat{H}_1 &= \sum_{i=1}^N \hat{\sigma}_i^x. \end{aligned} \quad (19)$$

The Kac-norm of $2/(N-1)$ arises from the choice to maintain the extensivity of the interaction energy. The Hamiltonian in equation 18 commutes with $P_{ij} \equiv \frac{1}{2} (1 + \vec{\sigma}_i \cdot \vec{\sigma}_j)$. In addition, it also commutes with the total angular momentum $S^2 = |\vec{S}|^2$, where $\vec{S} =$

$S^x \hat{x} + S^y \hat{y} + S^z \hat{z} \equiv \frac{1}{2} \sum_i \vec{\sigma}_i$. We now choose to populate the system in a state with $S^2 = \frac{N}{2} \left(\frac{N}{2} + 1 \right)$.

In that case, the dynamics remains invariant in the $N+1$ -dimensional space spanned by the common eigenstates of P_{ij} , $|S|^2$ and S_z ; the so-called *Totally Symetric Subspace*, or TSS [54]. Let the eigenvalues of S^z in the TSS be s_n , and the eigenvectors be $|s_n\rangle$. Here, $s_n = -\frac{1}{2} + \frac{n}{N}$ and the index $n = 0(1)N$ has $N+1$ values. The dynamics is restricted to this invariant subspace, wherein the matrix elements of the Hamiltonian are given by

$$\begin{aligned} \langle s_i | \hat{H}_0 | s_j \rangle &= -\frac{4}{N-1} s_i^2 \delta_{ij}, \\ \langle s_i | \hat{H}_1 | s_j \rangle &= \left[\sqrt{\frac{N}{2} \left(\frac{N}{2} + 1 \right)} - N s_i (N s_{i+1}) \delta_{i+1,j} \right. \\ &\quad \left. + \sqrt{\frac{N}{2} \left(\frac{N}{2} + 1 \right)} - N s_i (N s_{i-1}) \delta_{i-1,j} \right]. \end{aligned} \quad (20)$$

³¹⁴ These allow for a numerical representation of the
³¹⁵ Hamiltonian in the TSS.

³¹⁶ Next, we transform the Hamiltonian to the rotated
³¹⁷ frame given by the operator

$$\hat{U}(t) = \exp \left[i \frac{h}{\omega} \sin(\omega t) \hat{H}_1 \right]. \quad (21)$$

³¹⁸ This is analogous to the rotation performed for the
³¹⁹ TFIM in eqns 10 and 11. Defining $\tau = \frac{h}{\omega} \sin \omega t$, we use
³²⁰ the fact that $\hat{H}_1 = 2S^x$, as well as the following iden-
³²¹ tity obtained by using the Baker-Campbell-Hausdorff
³²² formula,

$$e^{i2\tau \hat{S}^x} \hat{S}^z e^{-i2\tau \hat{S}^x} = \hat{S}^z \cos(2\tau) + \hat{S}^y \sin(2\tau), \quad (22)$$

to simplify the transformed Hamiltonian $\tilde{H}(t) = \hat{U}^\dagger(t) \hat{H}(t) \hat{U}(t) - \hat{U}^\dagger(t) \partial_t \hat{U}(t)$, yielding

$$\begin{aligned} \tilde{H}(t) &= -\frac{1}{N-1} \left[(S^z)^2 (1 + \cos 4\tau) + (S^y)^2 (1 - \cos 4\tau) \right. \\ &\quad \left. + \{S^y, S^z\} \sin 4\tau \right] - 2h_0 S^x. \end{aligned} \quad (23)$$

³²³ Next, we define $\eta \equiv 4h/\omega$ and use the Jacobi-Anger
³²⁴ formula in eqn 12 to expand $\tilde{H}(t)$. This yields

$$\tilde{H}(t) = -\frac{\hat{S}^2}{N-1} + \frac{(\hat{S}^x)^2}{N-1} - 2h_0\hat{S}^x - \frac{J_0(\eta)}{N-1} \left[(\hat{S}^z)^2 - (\hat{S}^y)^2 \right] - \frac{2}{N-1} \left[(\hat{S}^z)^2 - (\hat{S}^y)^2 \right] \sum_{k=1}^{\infty} J_{2k}(\eta) \cos(2k\omega t) - \frac{2}{N-1} \{ \hat{S}^y, \hat{S}^z \} \sum_{k=1}^{\infty} J_{2k-1}(\eta) \sin[(2k-1)\omega t]. \quad (24)$$

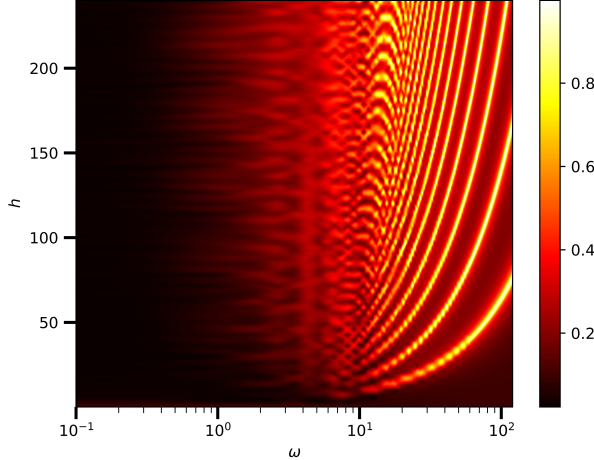


FIG. 3. Plot of the numerically averaged IPR (IPR computed using eqn 27) in the TSS plotted in the $h - \omega$ plane for $N = 100$ spins. In order to display the thermalized region more clearly, ω is plotted on a logarithmic scale on the abscissa. Note that, since the IPR is clearly non-negative, an average IPR of zero means that all Floquet states have zero IPR. Furthermore, the boundedness of IPR in $\phi_{IPR}(n) \leq 1$ ensures that if the average IPR is unity, then all Floquet states have unit IPR.

If ω is large enough to smooth out the harmonic components, we obtain the RWA,

$$\tilde{H}(t) \approx \tilde{H}_{\text{RWA}} \equiv -\frac{\hat{S}^2}{N-1} + \frac{(\hat{S}^x)^2}{N-1} - 2h_0\hat{S}^x - \frac{J_0(\eta)}{N-1} \left[(\hat{S}^z)^2 - (\hat{S}^y)^2 \right]. \quad (25)$$

If the drive amplitude h is adjusted such that η lies at a root of $J_0(\eta)$ (the localization point), the RWA Hamiltonian is diagonal in the representation of the simultaneous eigenstates of transverse field \hat{S}^x , and S^2 , yielding an IPR of unity in that representation, similar to the TFIM in the previous section. Note however, that if the DC transverse field h_0 is set to 0, then, at the localization point, the RWA Hamiltonian $\tilde{H}_{\text{RWA}} \sim (\hat{S}^x)^2$ in the TSS. The eigenvalues are two-fold degenerate. This produces infinitely many (Floquet) eigenmodes in the degenerate subspace whose IPRs may not always

be unity in the S^x representation. The removal of this degeneracy necessitates the inclusion of the d.c. field h_0 . However, note that rational values of h_0 may add accidental degeneracies in \tilde{H}_{RWA} . To see this, note that, at a localization point, the eigenvalues of \tilde{H}_{RWA} in the TSS are given by

$$\text{Eigs}\left[\tilde{H}_{\text{RWA}}\right] = \frac{\left(\frac{N}{2} - m\right)^2}{N-1} - 2h_0\left(\frac{N}{2} - m\right), \quad (26)$$

where the half-integer $-N/2 \leq m \leq N/2$ is the eigenvalue corresponding to a particular eigenstate $|m\rangle$ of the symmetry-breaking field \hat{S}^x . In order to ensure that no additional degeneracies occur, we have to set h_0 in such a way that no two energies accidentally coincide. If $N \gg 1$ (substantially large), then this condition can be readily met by assuring that $(1 - 2h_0)^{-1}$ is never an integer that is divisible by N . To ensure this in our numerical simulations, we have kept h_0 at a small irrational value. The localization of the Floquet states at resonance is supported by exact numerical results, as can be seen in the phase diagram fig 3. Here, we have plotted the arithmetic mean over all Floquet states of the IPR in the TSS for each point in the $h - \omega$ plane for $N = 100$ spins. The IPR in S^x representation is

$$\phi_{IPR}(n) = \sum_m |\langle m | \phi^n \rangle|^4. \quad (27)$$

As can be readily seen in the figure, the IPR is essentially zero when $\omega \lesssim 1$. There is considerable structure in the phase diagram for larger drive frequencies, and along the lines given by the roots of $J_0(\eta)$, the IPR is essentially unity, in agreement with eqn. 25.

In figure 4, we show plots of the IPR of the Floquet modes $|\phi^n\rangle$ for $S^2 = (N/2)(N/2+1)$. These plots were obtained numerically by diagonalizing the propagator $U(t)$ at $t = T$, where $U(t)$ is defined in eqn 5. This propagator was obtained from simulations of the exact quantum dynamics using QuTiP, the Quantum Toolbox in Python [55]. We kept the frequency at a fairly large value $\omega = 90$ where we expect that RWA would be valid, and $N = \mathcal{O}(10^2)$. The density plot in the upper panel of fig 4 depicts the IPR of the Floquet states; the abscissa $\eta = 4h/\omega$ and the ordinate is $n/(2N+1)$, where $n \leq 2N$ is a non-negative integer

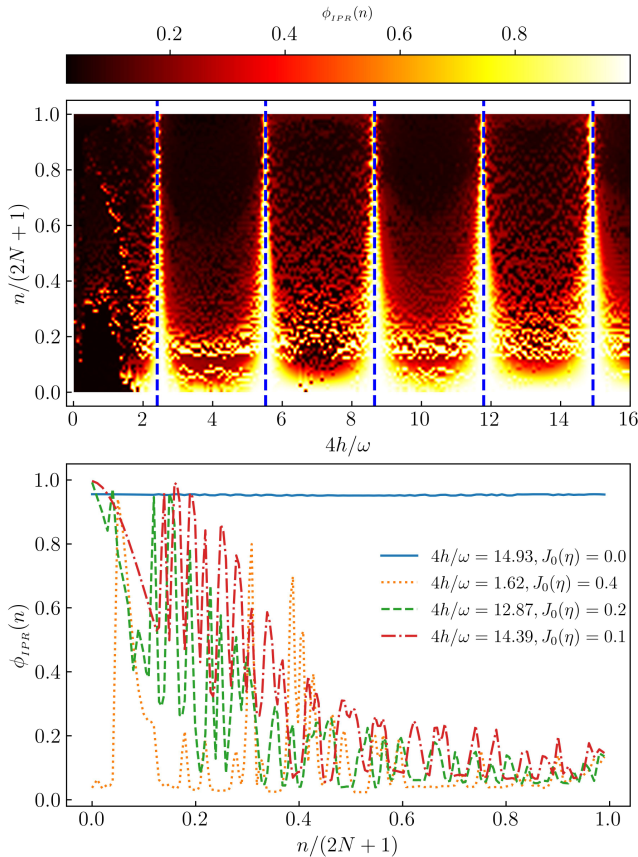


FIG. 4. IPR density plot for all possible Floquet modes (top panel ordinate) for different values of $\eta = 4h/\omega$ (top panel abscissa), deduced from equation 27 for exact LMG Hamiltonian for $N = 50$. Blue dashed lines are roots of $J_0(\eta)$. At bottom panel cross-section of IPR (ordinate)for four different η 's plotted for all possible floquet modes(bottom panel, abscissa) at $\omega = 90$. IPR founds to be \sim unity for all Floquet modes at roots of J_0 .

377 that indexes the Floquet states in increasing order of
378 m . The dashed vertical lines correspond to the roots
379 of $J_0(\eta)$. Comparing with the IPR of the TFIM in fig 1,
380 we can see a very similar patterns in the immediate
381 neighbourhood of the roots. Evidently, the IPR ap-
382 proaches a value of one for sufficiently large values of
383 the roots, strongly suggesting full DMBL. Deviations
384 occur at the smallest root of $J_0(\eta)$ (around $\eta = 2.405$).
385 due to the contributions from higher order terms in
386 eq 24. Thus, a higher root is favored for DMBL.

387 The bottom panel of fig 4 contains cross sections
388 of the full IPR plot for selected values of η as indi-
389 cated in the legend. When the drive amplitude h is
390 adjusted such that η is close to a root of $J_0(\eta)$, the Flo-
391 quet States are mixed, but not entirely thermal, since
392 the IPR does not fall to $\mathcal{O}(N^{-1})$, indicating that local-
393 ization persists to some extent. However, the further
394 we are from the roots, the closer the IPR gets to one
395 predicted by thermalization.

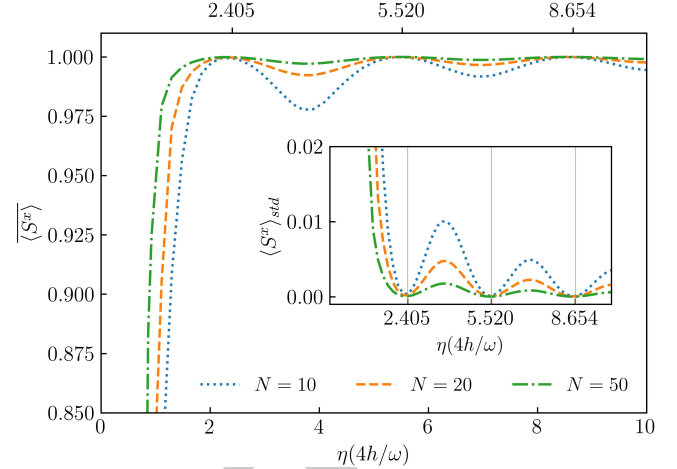


FIG. 5. Temporal average of $\langle \hat{S}^x \rangle$ (ordinate) for different η 's (abscissa) is plotted for $\sim 200T$ at higher ω for different $N=10, 20, 50$. $\langle \hat{S}^x \rangle$ is found to be unity at roots of $J_0(\eta)$. At points away from resonance points, $\langle \hat{S}^x \rangle$ falls below unity. The corresponding standard deviation $\langle \hat{S}^x \rangle_{std}$ supports the variation of $\langle \hat{S}^x \rangle$ (inset fig.). $\langle \hat{S}^x \rangle_{std}$ is ~ 0 describing a full freezing of the system at roots of $J_0(\eta)$ (red vertical solid lines).

396 Figure 5 shows plots of the long-time average (from
397 $t = 0 - 200T$) of the field amplitude $\langle \hat{S}^x \rangle$ as a function
398 of η . The system is started from the fully polarized
399 state $s_n = N/2$ in the TSS and the dynamics simulated.
400 The average is plotted for different values of ampli-
401 tude h , keeping the frequency fixed at a high value of
402 $\omega = 90$. It is clearly very close to unity at roots of $J_0(\eta)$
403 and falls at points away from it, indicating that S^x is
404 approximately conserved at the localization points.

405 Small deviations do occur due to the role of higher
406 order terms in the rotated Hamiltonian in eq 23. This
407 can be demonstrated quantitatively by comparing the
408 IPR obtained from the exact dynamics simulation with
409 that obtained from the dynamics of $\tilde{H}(t)$ in eq. 23 after
410 truncating the series at orders $k \geq 1$. This compari-
411 son can be seen in fig 6. The IPR plots from the ex-
412 act dynamics indicate that the first localization point,
413 represented by the lowest root of $J_0(\eta)$, does not show
414 complete DMBL. However, DMBL is particularly con-
415 spicuous at large roots. The IPRs of the Floquet states
416 obtained from the RWA dynamics exhibit large devia-
417 tions from unity when away from the localization point
418 as evidenced by the green and red curves in the mid-
419 dle panel of fig 6. However, complete localization is
420 seen in the RWA dynamics at any localization point, in
421 contrast to the exact case in the top panel. Thus, it
422 is necessary to incorporate higher-order corrections
423 into the Rotating Wave Approximation (RWA) at lower

429 III. PERSISTENCE OF DMBL IN THE CONTINUUM
430 LIMIT

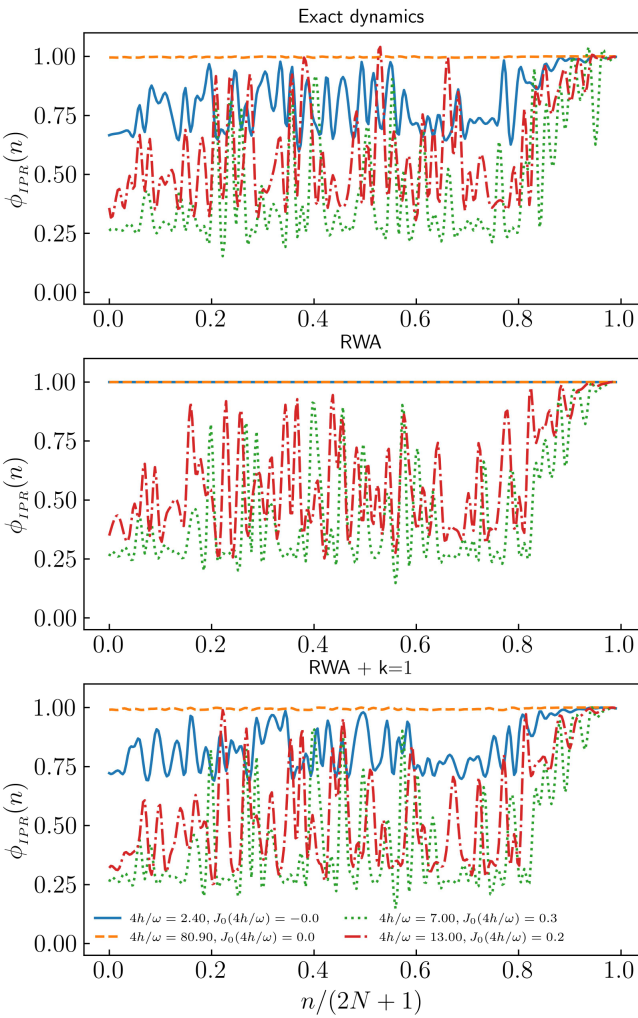


FIG. 6. The comparison between IPR for exact dynamics and RWA with corresponding correction orders. IPR is calculated for four different η 's and corresponding $J_0(\eta)$ values for colors, Blue : $\eta = 2.40, J_0(\eta) = 0.0$, dashed orange: $\eta = 80.9, J_0(\eta) = 0.0$, Green: $\eta = 7.0, J_0(\eta) = 0.3$, Red: $\eta = 13, J_0(\eta) = 0.2$. At low root of $J_0(\eta)$ IPR is not unity (Blue curve) while at higher root (orange dashed) it is unity while at points away from roots IPR are less than unity in the exact (top panel) plot. RWA does not matches with the exact plot. At all roots of $J_0(\eta)$ IPR is unity(middle panel). RWA with additional higher order terms exhibit similar system pattern(Bottom panel) with exact dynamics.

425 localization points. The application of the first-order
426 correction to RWA in the lower panel of fig 6 results in
427 a curve structure that is closer to that from the exact
428 dynamics.

431 In the continuum limit, where $N \rightarrow \infty$, the disparity
432 between neighboring values of s_i in equation 20 can
433 be disregarded, and s_i can be mapped to a continuum
434 $q \in [-1/2, 1/2]$ [54]. We define the Hamiltonian per
435 particle $h(t) \equiv \frac{H(t)}{N}$, and a canonically conjugate co-
436 ordinate $Np \equiv \left\langle -i \frac{\partial}{\partial q} \right\rangle$. Then, in this limit, the dynam-
437 ics can be approximated by that of a classical Hamil-
438 tonian [56]

$$h(t) = -2q^2 - [h \cos \omega t + h_0] \sqrt{1 - 4q^2} \cos p, \quad (28)$$

which yields the dynamical system

$$\begin{aligned} \frac{dq}{dt} &= \frac{\partial h}{\partial p} = h(t) \sqrt{1 - 4q^2} \sin p \\ \frac{dp}{dt} &= -\frac{\partial h}{\partial q} = 4q \left[1 - \frac{h(t) \cos p}{\sqrt{1 - 4q^2}} \right], \end{aligned} \quad (29)$$

439 where $h(t) = [h \cos \omega t + h_0]$. We have profiled simu-
440 lations of the ensuing dynamics with the *Poincaré sur-*
441 *face of section* (PSOS) of the full dynamics. Here, the
442 (q, p) -phase space is strobed at $t = nT$, and plotted
443 for a large number of initial conditions. The results
444 are shown in the upper panels of fig 7 for a small value
445 of $\omega = 2.0$ (left panel) and a large value $\omega = 90$ (right
446 panel). In both cases, the value of h is chosen such
447 that η lies on the first root of $J_0(\eta)$. The onset of chaos
448 for small drive frequency indicates thermal behaviour
449 for typical initial conditions, with small islands of reg-
450 ularity for others. This is consistent with similar re-
451 sults for small frequencies reported in [52, 57]. How-
452 ever, at high frequency, the regular islands distinctly
453 dominate over the chaos. The trajectories indicate
454 that the conservation of $\langle S^x \rangle \approx \sqrt{1 - 4q^2} \cos p$ [54]
455 at high ω persists in the thermodynamic limit. That
456 this is a signature of the underlying quantum dynam-
457 ics can be readily seen in the quantum phase space
458 representation of the Floquet Eigenstates for a large
459 but finite N . These are shown in the correspondingly
460 lower panels of fig 7. Here, we have plotted the Spec-
461 tral Average of the Husimi Q-functions of the acquired
462 Floquet States in the TSS. Specifically, for a coher-
463 ent state $|q, p\rangle$, the corresponding Spectral-Averaged
464 Husimi distribution [58] is obtained by

$$H(q, p) \equiv \frac{1}{(2N+1)\pi} \sum_n \langle q, p | \phi^n \rangle \langle \phi^n | q, p \rangle. \quad (30)$$

465 The quantum phase space retains signatures of the
466 classical phase space dynamics when $N = 100$, indi-
467 cating the onset of the persistence of S^x conservation
468 that arises from the resonance condition at high fre-
469 quencies.

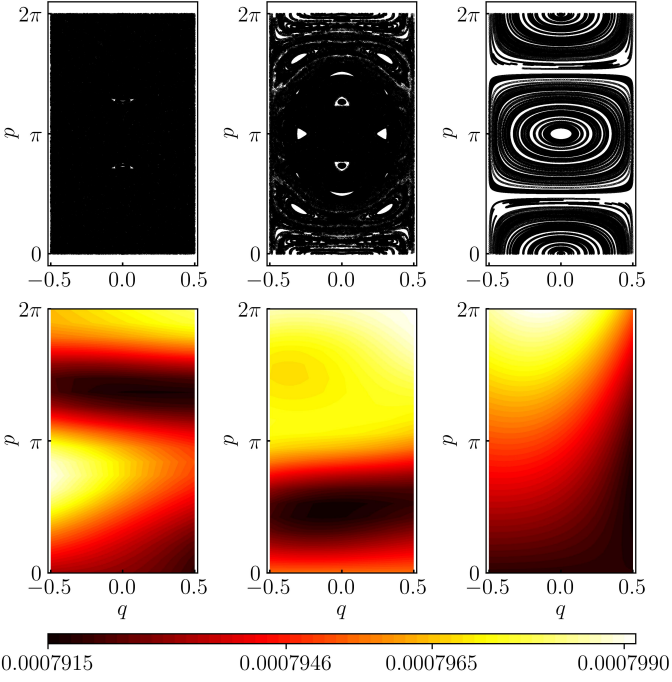


FIG. 7. Phase-space distributions at $\omega = 1.0$ (left panels), $\omega = 2.5$ (middle panels) and $\omega = 90.0$ (right panels) for 100 initial conditions. The drive amplitude h is always adjusted such that $\eta = 4h/\omega$ lies on the smallest root of $J_0(\eta)$, i.e. $\eta = 2.4048\dots$. At small $\omega = 1.0$, the classical PSOS, obtained from simulating the dynamics in eqns 29 (top left panel), shows chaotic behaviour, and at $\omega = 2.5$, regular regions start to appear. At higher $\omega = 90.0$, the dominance of regular dynamics can be readily seen (top right panel). The bottom panels plot the corresponding Spectral-Averaged Husimi-Q function, obtained from the Floquet modes $|\phi^n\rangle$ using eqn. 30, and setting $N = 100$. The $\omega = 1.0$ case (bottom left panel) has a dispersed distribution in colour. This is consistent with the chaotic behaviour seen in the continuum limit. At $\omega = 2.5$ (bottom middle panel), there is a partial regular pattern observed together with a dispersed pattern. In the $\omega = 90$ -case (bottom right panel), the distribution has distinct colour contrasts, which is consistent with the regular dynamics pattern seen in the continuum limit.

471 IV. PHASE CROSSOVER FROM THERMAL TO DMBL

472 The analysis of the periodically driven LMG model
473 reveals two distinct scenarios at low and high external
474 drive frequencies. In the former case, thermalization
475 in accordance with FETH is seen, whereas in the latter
476 case, DMBL is induced. As a result, we hypothesize
477 that a macroscopic change in phase occurs due to the
478 influence of frequency.

479 To demonstrate this, we investigate the IPR of the
480 Floquet mode with smallest quasienergy for numer-
481 ous frequencies and system sizes, along with the as-
482 sociated drive amplitude h keeping the system at a lo-
483 calization point. The results are shown in fig 8. In the

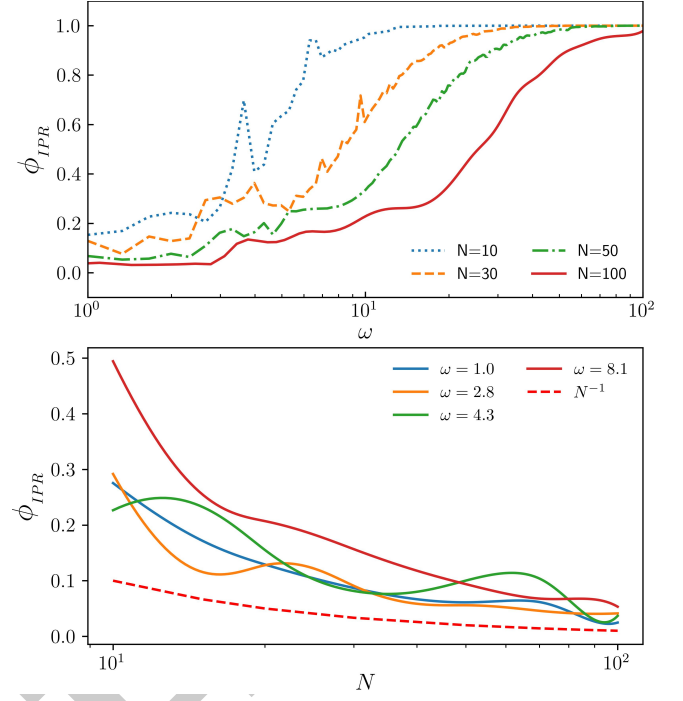


FIG. 8. In the top panel, the IPR of the lowest quasienergy Floquet state is plotted as a function of ω for different N s, with amplitude h adjusted to ensure that $J_0(\eta) = 0$ always. The smooth rise in IPR defines a phase crossover (top panel) between a fully thermal phase to a fully localized phase. The bottom panel plots the IPR versus N for small ω s, also with h adjusted. The curves asymptotically approach the dependency $\phi_{IPR} \sim 1/N$, indicating thermalization at low- ω .

484 low-frequency range $\omega \in [1.0, 9.0]$, the IPR exhibits val-
485 ues well below unity. Moreover, the IPR gradually di-
486 minishes with increasing system size, following a sys-
487 tem-size inverse proportional trend. Moreover, as can
488 be seen in the bottom panel of the same figure, when
489 the dynamics is simulated for smaller ω s, the fall of
490 $\phi_{IPR}(N)$ asymptotically approaches one that charac-
491 terizes a fully thermal state, where $\phi_{IPR}(N) \sim 1/N$
492 in the TSS. This confirms the participation distribu-
493 tion (as shown in the bottom panel). As In the limit
494 $N \rightarrow \infty$, the inverse participation ratio (IPR) tends to
495 towards zero, indicating a fully de-localized state. Con-
496 trast this with the IPR plots shown in the bottom left
497 panel of fig 2 for the integrable TFIM. The plots reveal
498 The top panel of fig. 8 also reveals a gradual increase
499 in the unity towards unity of IPR over a certain fre-
500 quency range, specifically at $\omega \approx 5$. In addition, the
501 rise does not cross with those for different values of
502 N , suggesting the onset of a phase crossover [42, 59].
503 As the size of the system increases, the crossover re-
504 gion becomes smoother, rather than sharper.

505 We can also look at this crossover more clearly in
506 the plots of the heating rate of the system, defined
507 simply by the expectation value of the Hamiltonian,

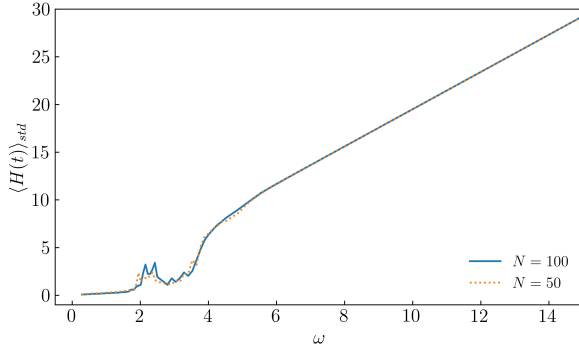


FIG. 9. The standard deviation of the heating rate, denoted by $\langle H \rangle_{std}$, calculated over a span of $t = 500T$ for two system sizes. Here, h is varied to keep $\eta = 4h/\omega$ at the first root of $J_0(\eta)$. A nonsingular rise has been identified at $\omega \approx 4.0$. $\langle H \rangle_{std}$ exhibits a diminutive magnitude below that value of ω , while a linear rise is observed at higher frequencies, consistent with freezing. A vanishingly small standard deviation for $\omega \ll 4.0$ indicates the presence of a thermal region, whereas a larger finite standard deviation suggests the existence of athermal behaviour. The small peaks observed at $\omega \in [2, 4]$ are finite-size effects that disappear in the thermodynamic limit.

510 $\langle \hat{H}(t) \rangle$. We have carried out the numerical evalua-
 511 tion from the simulated dynamics over $t = 500T$.
 512 When the system is adequately described by FETH,
 513 the temporal fluctuations in the Hamiltonian, defined
 514 by $\langle H \rangle_{std}^2 \equiv \overline{\langle \hat{H} \rangle^2} - \overline{\langle \hat{H} \rangle}^2$ (see eqn 3), are minimal in
 515 the thermodynamic limit, as the spread of states leads
 516 to a limited standard deviation[60]. Conversely, the
 517 onset of athermality is indicated by nonzero fluctua-
 518 tions in time. If we set the initial state to the fully po-
 519 larized state in the TSS (given by $|s_N\rangle$), then the onset
 520 of freezing, together with DMBL, will result in nearly
 521 infinite hysteresis in the ensuing dynamics, causing
 522 $|\psi\rangle(t) \approx |s_N\rangle \forall t$. From eqn. 18, we can clearly see
 523 that this will lead to a linearly rising dependence on
 524 ω in $\langle H \rangle_{std}$ as long as we stick to a localization point
 525 given by a fixed h/ω [61]. All these observations are
 526 corroborated by the heating rate plots in figure 9.

527

V. CONCLUSION AND OUTLOOK

528 We have delved into the onset of freezing and
 529 phase cross-over in 1D spin systems driven by a time-
 530 periodic transverse field, contrasting the responses
 531 in the Transverse Field Ising Model (TFIM) with that
 532 of the long-range Lipkin-Meshkov-Glick Model (LMG).
 533 The parametrization of DMBL is based on the Inverse
 534 Participation Ratio (IPR) of the Floquet eigenstates.
 535 Our investigations compared the IPRs from both mod-

536 els numerically, and found the emergence of thermal
 537 behavior at low frequencies and freezing at high fre-
 538 quencies for the LMG model, the latter a direct conse-
 539 quence of the appearance of additional approximately
 540 conserved quantities.

541 Long-range spins exhibit strong localization in spin-
 542 coordinate space for the LMG model when the drive
 543 frequency is $\omega \gg J$, where J represents the spin ex-
 544 change energy. The localization of the LMG model
 545 occurs at specific resonance points of the drive fre-
 546 quency ω and amplitude h , at $J_0(4h/\omega) = 0$, $\omega \gg J$.
 547 This is apparently similar to the phenomenon of Dy-
 548 namical Freezing (DMF) in the Transverse Field Ising
 549 Model (TFIM), where comparable localization at res-
 550 onance points, determined by the roots of $J_0(2h/\omega)$,
 551 occurs due to the onset of an additional approximate
 552 conservation in the transverse field itself. However,
 553 a key difference is the thermal behaviour of the LMG
 554 model at low frequencies. Plots of the IPR for a range
 555 of frequencies along the resonance manifold exhibits
 556 a smooth increase in IPR yielding a quantum phase-
 557 crossover from a thermal phase governed by the Flo-
 558 quet Eigenstate Thermalization Hypothesis (FETH) to
 559 a Dynamically Many-Body localized phase (DMBL).
 560 This crossover is absent in the TFIM, as can be readily
 561 seen in the significant magnitude of the inverse par-
 562 ticipation ratio (IPR) even at low frequencies. Thus,
 563 the suppression of thermalization through Dynamical
 564 Many Body Localization in long-range systems can be
 565 controlled via Floquet engineering, even in clean sys-
 566 tems without any disorder. Thus, periodically driven
 567 long-range spin systems are an excellent tool for in-
 568 vestigating disorder-free Many Body Localization, as
 569 can be readily seen via the IPR of its Floquet modes.
 570 There are several unexplored indicators of DMBL,
 571 such as entanglement entropy and level statistics [10],
 572 which we defer to future studies. In addition,
 573 Halpern in 2019 proposed a quantum engine based
 574 on MBL[11] which works between strong localized
 575 and thermal phases of the system. In our proposed
 576 LMG model, tuning the system parameters by bring-
 577 ing them to the resonance points, then adiabatically
 578 cycling the frequency from the thermal region to the
 579 DMBL region, can achieve a similar engine without
 580 going through a phase transition.

A. Acknowledgements:

581 MR acknowledges The University of Burdwan for
 582 support via a state-funded fellowship. AR acknowl-
 583 edges support from the University Grants Commission
 584 (UGC) of India, Grant No. F.30-425/2018(BSR), as well
 585 as from the Science and Engineering Research Board
 586 (SERB), Grant No. CRG/2018/004002.

- [1] P. Bordia, H. Lüschen, U. Schneider, M. Knap, and I. Bloch, Nat. Phys. **13**, 460 (2017).
- [2] S. Sahoo, I. Schneider, and S. Eggert, (2019), arXiv:1906.00004 [cond-mat.str-el].
- [3] A. Das, Phys. Rev. B **82**, 172402 (2010).
- [4] G. B. Mbeng, A. Russomanno, and G. E. Santoro, (2020), arXiv:2009.09208 [quant-ph].
- [5] H. S. Yamada and K. S. Ikeda, Phys. Rev. E **105**, 054201 (2022).
- [6] A. Roy and A. Das, Phys. Rev. B **91**, 121106 (2015).
- [7] H. Li, B. Shapiro, and T. Kottos, Phys. Rev. B **98**, 121101 (2018).
- [8] A. Eckardt and E. Anisimovas, New J. Phys. **17**, 093039 (2015).
- [9] L. Zhang, V. Khemani, and D. A. Huse, Phys. Rev. B **94**, 224202 (2016).
- [10] V. Khemani, A. Lazarides, R. Moessner, and S. L. Sondhi, Phys. Rev. Lett. **116**, 250401 (2016).
- [11] N. Yunger Halpern, C. D. White, S. Gopalakrishnan, and G. Refael, Phys. Rev. B **99**, 024203 (2019).
- [12] T. Nag, S. Roy, A. Dutta, and D. Sen, Phys. Rev. B **89**, 165425 (2014).
- [13] G. Carleo, F. Becca, M. Schiró, and M. Fabrizio, Sci. Rep. **2**, 243 (2012).
- [14] S. Aditya and D. Sen, (2023), arXiv:2305.06056 [cond-mat.stat-mech].
- [15] M. Schiulaz, A. Silva, and M. Müller, Phys. Rev. B **91**, 184202 (2015).
- [16] T. Grover and M. P. A. Fisher, J. Stat. Mech. Theory Exp. **2014**, P10010 (2014).
- [17] Z. Papić, E. M. Stoudenmire, and D. A. Abanin, Ann. Physics **362**, 714 (2015).
- [18] A. Smith, J. Knolle, D. L. Kovrizhin, and R. Moessner, Phys. Rev. Lett. **118**, 266601 (2017).
- [19] O. Hart, S. Gopalakrishnan, and C. Castelnovo, Phys. Rev. Lett. **126**, 227202 (2021).
- [20] H. Lipkin, N. Meshkov, and A. Glick, Nuclear Phys. B **62**, 188 (1965).
- [21] N. Meshkov, A. Glick, and H. Lipkin, Nuclear Phys. B **62**, 199 (1965).
- [22] A. Glick, H. Lipkin, and N. Meshkov, Nuclear Phys. B **62**, 211 (1965).
- [23] P. Ribeiro, J. Vidal, and R. Mosseri, Phys. Rev. E **78**, 021106 (2008).
- [24] N. Debergh and F. Stancu, J. Phys. A: Math. Gen. **34**, 3265 (2001).
- [25] P. Titum and M. F. Maghrebi, Phys. Rev. Lett. **125**, 040602 (2020).
- [26] A. Campa, T. Dauxois, and S. Ruffo, Phys. Rep. **480**, 57 (2009).
- [27] T. Eisele and R. S. Ellis, J. Stat. Phys. **52**, 161 (1988).
- [28] A. Canning, Physica A **185**, 254 (1992).
- [29] D. Vu, K. Huang, X. Li, and S. Das Sarma, Phys. Rev. Lett. **128**, 146601 (2022).
- [30] G. Misguich, V. Pasquier, and J.-M. Luck, Phys. Rev. B **94**, 155110 (2016).
- [31] M. Calixto and E. Romera, J. Stat. Mech. Theory Exp. **2015**, P06029 (2015).
- [32] K. Fujii, Journal of Modern Physics **8**, 2042 (2017).
- [33] B. Sutherland, *Beautiful Models* (WORLD SCIENTIFIC, 2004) Chap. 2.
- [34] D. A. Abanin, E. Altman, I. Bloch, and M. Serbyn, Rev. Mod. Phys. **91**, 021001 (2019).
- [35] M. Srednicki, Phys. Rev. E **50**, 888 (1994).
- [36] M. Srednicki, J. Phys. A: Math. Gen. **32**, 1163 (1999).
- [37] M. Holthaus, J. Phys. B: At. Mol. Opt. Phys. **49**, 013001 (2015).
- [38] M. Vogl, M. Rodriguez-Vega, and G. A. Fiete, Phys. Rev. B **101**, 024303 (2020).
- [39] M. Bükov, L. D'Alessio, and A. Polkovnikov, Adv Phys **64**, 139 (2015).
- [40] L. D'Alessio and M. Rigol, Phys. Rev. X **4**, 041048 (2014).
- [41] R. Yousefjani, S. Bose, and A. Bayat, Phys. Rev. Res. **5**, 013094 (2023).
- [42] P. Sierant, M. Lewenstein, A. Scardicchio, and J. Zakrzewski, Phys. Rev. B **107**, 115132 (2023).
- [43] F. Alet and N. Laflorencie, C. R. Phys. **19**, 498 (2018).
- [44] S. J. Garratt and S. Roy, Phys. Rev. B **106**, 054309 (2022).
- [45] R. B. Stinchcombe, J. Phys. C: Solid State Phys. **6**, 2459 (1973).
- [46] F. E. H. George Arfken, Hans Weber, *Mathematical Methods for Physicists*, 7th ed. (Academic Press, 2011).
- [47] S. Mukherjee, A. Spracklen, D. Choudhury, N. Goldman, P. Öhberg, E. Andersson, and R. R. Thomson, New J. Phys. **17**, 115002 (2015).
- [48] S.-H. Lin, B. Sbierski, F. Dorfner, C. Karrasch, and F. Heidrich-Meisner, SciPost Phys. **4**, 002 (2018).
- [49] N. C. Murphy, R. Wortis, and W. A. Atkinson, Phys. Rev. B **83**, 184206 (2011).
- [50] E. J. Torres-Herrera, I. Vallejo-Fabila, A. J. Martínez-Mendoza, and L. F. Santos, Phys. Rev. E **102**, 062126 (2020).
- [51] N. Trivedi and D. Heidarian, Prog. Theor. Phys. Suppl. **160**, 296 (2005).
- [52] A. Russomanno, R. Fazio, and G. E. Santoro, Europhys. Lett. **110**, 37005 (2015).
- [53] N. Defenu, T. Enss, M. Kastner, and G. Morigi, Phys. Rev. Lett. **121**, 240403 (2018).
- [54] T. Mori, J. Phys. A: Math. Theor. **52**, 054001 (2019).
- [55] J. Johansson, P. Nation, and F. Nori, Comput. Phys. Commun. **184**, 1234 (2013).
- [56] B. Sciolla and G. Biroli, Phys. Rev. Lett. **105**, 220401 (2010).
- [57] R. A. Kidd, M. K. Olsen, and J. F. Corney, Phys. Rev. A **100**, 013625 (2019).
- [58] A. Bäcker, S. Fürstberger, and R. Schubert, Phys. Rev. E **70**, 036204 (2004).
- [59] S. Sachdev, *Quantum Phase Transitions*, 2nd ed. (Cambridge University Press, Cambridge, 2011).
- [60] P. Reimann, J. Stat. Mech. Theory Exp. **2021**, 103106 (2021).

⁷⁰² [61] When frozen, $|\psi(t)\rangle \approx |s_N\rangle$. From eqn 18, $\langle \hat{H}_{0,1} \rangle$ are
⁷⁰³ both approx. constant. Averaging the square of $\langle \hat{H}(t) \rangle$

⁷⁰⁴ over long times yields dependency $\sim h^2 + \delta$, where $\delta \sim$
⁷⁰⁵ $h_0 \ll 1$. Thus, the std. devn. in time $\sim h \sim \omega$, since
⁷⁰⁶ $\eta = 4h/\omega$ is kept fixed.

DRAFT